The Astrophysical Journal Letters, 929:L9 (7pp), 2022 April 10 https://doi.org/10.3847/2041-8213/ac62cc

The Archival Discovery of a Strong Lyα and [C II] Emitter at $z = 7.677$

Francesco Valentino[1,2], Gabriel Brammer[1,2], Seiji Fujimoto[1,2], Kasper E. Heintz[1,2,3], John R. Weaver[1,2], Victoria Strait[1,2], Katriona M. L. Gould[1,2], Charlotte Mason[1,2], Darach Watson[1,2], Peter Laursen[1,2], and Sune Toft[1,2]
[1] Cosmic Dawn Center (DAWN), Denmark; francesco.valentino@nbi.ku.dk
[2] Niels Bohr Institute, University of Copenhagen, Jagtvej 128, DK-2200 Copenhagen N, Denmark
[3] Centre for Astrophysics and Cosmology, Science Institute, University of Iceland, Dunhagi 5, 107 Reykjavík, Iceland
Received 2022 March 7; revised 2022 March 30; accepted 2022 March 30; published 2022 April 11

Abstract

We report the archival discovery of Lyα emission from the bright ultraviolet galaxy Y002 at $z = 7.677$, spectroscopically confirmed by its ionized carbon [C II] 158 μm emission line. The Lyα line is spatially associated with the rest-frame UV stellar emission ($M_{\rm UV} \sim -22$, $2\times$ brighter than $M^{\star}_{\rm UV}$), and it appears offset from the peak of the extended [C II] emission at the current $\sim 1''$ spatial resolution. We derive an estimate of the unobscured $\rm SFR_{UV} = (22 \pm 1)\ M_{\odot}\ yr^{-1}$ and set an upper limit of $\rm SFR_{IR} < 15\ M_{\odot}\ yr^{-1}$ from the far-infrared (FIR) wavelength range, which globally places Y002 on the SFR(UV+IR)–$L_{\rm [C\ II]}$ correlation observed at lower redshifts. In terms of velocity, the peak of the Lyα emission is redshifted by $\Delta v_{\rm Ly\alpha} \sim 500$ km s^{-1} from the systemic redshift set by [C II] and a high-velocity tail extends up to $\sim$1000 km s^{-1}. The velocity offset is up to $\sim 3.5\times$ higher than the average estimate for similarly UV-bright emitters at $z \sim 6$–7, which might suggest that we are witnessing the merging of two clumps. A combination of strong outflows and the possible presence of an extended ionized bubble surrounding Y002 would likely facilitate the escape of copious Lyα light, as indicated by the large equivalent width $\rm EW_0(Ly\alpha) = 24^{+5}_{-6}$ Å. Assuming that [C II] traces the neutral hydrogen, we estimate a H I gas fraction of $M_{\rm H\ I}/M_{\star} \gtrsim 8$ for Y002 as a system and speculate that patches of high H I column densities could contribute to explaining the observed spatial offsets between Lyα- and [C II]-emitting regions. The low dust content, implied by the nondetection of the FIR continuum emission at rest frame $\sim$160 μm, would be sufficient to absorb any potential Lyα photons produced within the [C II] clump as a result of large H I column densities.

Unified Astronomy Thesaurus concepts: Lyman-alpha galaxies (978); Lyman-break galaxies (979); High-redshift galaxies (734); Reionization (1383); Galaxy evolution (594); Interstellar medium (847)

1. Introduction

The direct confirmation and the physical characterization of a large number of galaxies at $z > 6$–7 is an important step toward a complete understanding of the process of reionization of the intergalactic medium (IGM) at this epoch, its main drivers, timeline, and topology (Loeb & Barkana 2001; Dayal & Ferrara 2018). Thus far, the workhorses of the spectroscopic campaigns targeting high-redshift sources have been the Lyα emission (Lyα at 1215.67 Å) and, more recently, the bright far-infrared (FIR) cooling lines of ionized carbon ([C II] at 157.74 μm) and oxygen ([O III] at 51.82 and 88.36 μm). The combination of these lines from warm (Lyα, [O III]) and cold ([C II]) phases of the interstellar medium (ISM), together with the modeling of the stellar and dust-emitted light, also gives us the opportunity to start deciphering the earliest phases of galaxy growth. The resonant Lyα emission is a primary tool for investigation, being sensitive to the onset of star formation, its feedback on the surrounding ISM and IGM, and to what extent their main component, hydrogen, is neutral or ionized. The addition of nonresonant FIR transitions not only allows us to pinpoint the systemic redshifts inaccessible with Lyα, but offers a complementary insight into the metallicity, ionization, and dynamics of the ISM without being hampered by dust absorption as strongly as rest-frame optical lines. Moreover, their underlying FIR continuum emission tracks the first dust grains formed in the universe.

Scarce [C II] detections were initially reported for Lyα emitters at $z \gtrsim 5$ and interpreted as owing to the low metal content and high ionization rates expected in early galaxies (Vallini et al. 2015; Harikane et al. 2018). This would also be reflected in bright [O III] lines and large [O III]/[C II] ratios and was indeed reported (Hashimoto et al. 2019). Recent systematic searches for [C II] in large samples at $z \sim 4$–8 revealed a wide variety of galaxy properties and copious [C II] photons from Lyα emitters (e.g., Capak et al. 2015; Le Fèvre et al. 2020; Bouwens et al. 2021b; Endsley et al. 2022). This allowed for the first statistical assessments of the correlations underlying the Lyα and [C II] emission. Galaxies with large Lyα equivalent widths ($\rm EW_0(Ly\alpha)$) are found to correlate with a [C II] deficit compared with the UV emission—and, thus, SFR—at $z > 6$ (Carniani et al. 2018; Harikane et al. 2018; Hashimoto et al. 2019). This is in contrast with observations at $z \sim 4$–6 (Schaerer et al. 2020) where the difference might be driven by diverse sample selections, a possible redshift-dependent effect, and the large scatter in the properties of individual emitters (Harikane et al. 2020). The situation is further complicated by the observed clumpy structures and spatial offsets among the stellar light and gaseous or dusty components and even within different phases of the ISM (Bowler et al. 2017; Carniani et al. 2018). Therefore, the addition of new sources with multiple line transitions at the highest possible redshifts is still of primary importance to shed light on the earliest phases of galaxy formation and their impact on the surrounding IGM.

Here we report the detection of Lyα emission from archival data of a Lyman-break galaxy (LBG) at the extreme bright end of the luminosity function with confirmed [C II] emission at $z = 7.677$ in the COSMOS field, dubbed Y002 hereafter. This object has been indicated as a high-redshift photometric candidate (UVISTA-Y2 with $z_{\rm phot} = 8.21^{+0.49}_{-0.50}$; Stefanon et al. 2017, 2019), later followed up with the Atacama Large Millimeter/submillimeter Array (ALMA) in a pilot (Schouws et al. 2022) and then in the full Reionization Era Bright Emission Line Survey (REBELS-36 with $z_{\rm phot} = 7.88^{+0.58}_{-0.20}$; Bouwens et al. 2021b). We describe our archival search and independent data reduction in Section 2. The analysis of the derived properties and a discussion of the relevant findings in the context of the current research landscape are presented in Section 3, followed by conclusions in Section 4. We assume a ΛCDM cosmology with $\Omega_{\rm m} = 0.3$, $\Omega_\Lambda = 0.7$, and $H_0 = 70\,{\rm km\,s^{-1}\,Mpc^{-1}}$. All magnitudes are expressed in the AB system.

2. Data and Methods

2.1. Keck Near-infrared Spectroscopy

As part of a large archival effort, we reduced spectroscopic *Y*-band data for Y002 taken with the Keck Multi-Object Spectrometer For Infra-Red Exploration (MOSFIRE; McLean et al. 2012).[4] The target was observed for 3.5 hr on 2015 December 18, with an average seeing of FWHM $= 0\farcs89$. We applied the distributed pipeline for the data reduction followed by an optimal extraction of the 1D spectrum (Horne 1986). We corrected for minor telescope drifting and derived the flux calibration based on a star observed within the same mask and in the same conditions as Y002. Finally, we anchored the photometry to the latest UltraVISTA DR4 *Y*-band flux as part of the COSMOS2020 catalog (Weaver et al. 2022) to correct for further flux losses. We computed a reduced $\chi^2 = 1.0$ in regions of pure background in the 2D frame, confirming the reliability of the noise estimate. The 2D and 1D spectra are shown in Figure 1. We then modeled the Lyα line profile as a Gaussian curve in the spectrum at the original resolution ($\sim$31 km s^{-1} velocity bin at the redshifted Lyα wavelength). The best-fit parameters are reported in Table 1. We also attempted to use a skewed Gaussian curve to allow for a possible asymmetry in the Lyα profile (Figure 1), but without significantly improving the fit (the Akaike Information Criterion (AIC) criterion does not strongly favor either model: $\Delta{\rm AIC} = 1.25$, with a $\sim$50% probability that the skewed Gaussian is a better representation of the data).

2.2. ALMA Far-infrared Spectroscopy

Y002 was observed in Band 6 with ALMA as part of the REBELS survey and its pilots[5] (REBELS; Bouwens et al. 2021b; Schouws et al. 2022). The archival calibrated measurement set is provided by ESO, and we used the Common Astronomy Software Applications package (CASA; McMullin et al. 2007) to analyze the data. We combined the available data with CONCAT and produced a line cube and a continuum map with a pixel scale of $0\farcs1$ with TCLEAN, adopting a natural weighting scheme. The final beam size is $1\farcs59 \times 1\farcs29$, while we set a 30 km s^{-1} channel velocity width for the cube, sufficient to resolve typical emission lines at high redshift over several bins.

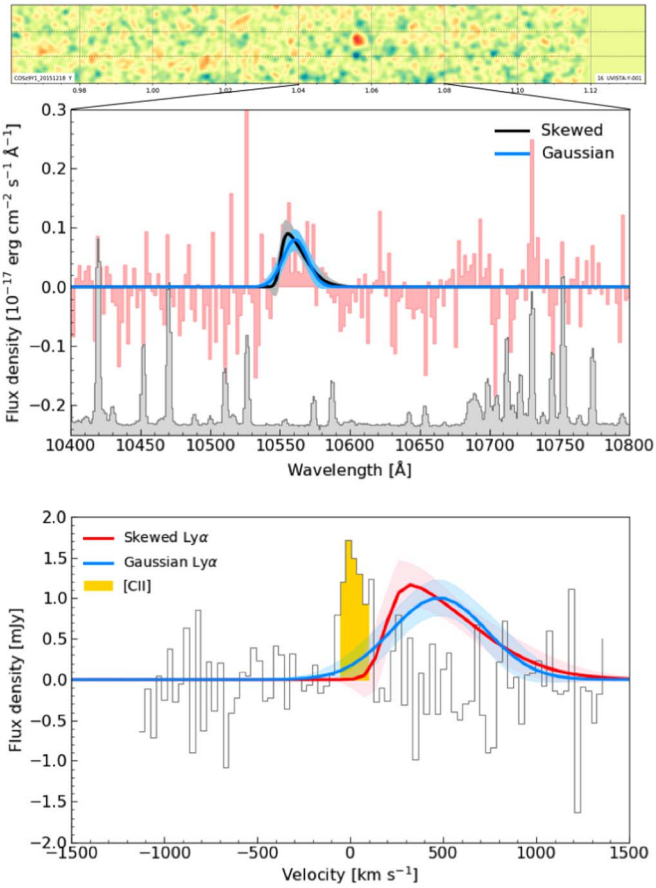

Figure 1. Top: bidimensional spectrum of Y002 smoothed with a Gaussian filter for display purposes. Center: the red and gray areas show the optimally extracted spectrum around the region of Lyα emission at $z = 7.677$ and the associated noise, binned by a factor of 2 for clarity. The blue and black lines and shaded areas indicate the best simple and skewed Gaussian models and their confidence intervals. Bottom: the ALMA Band 6 spectrum of Y002 where the velocity zero point corresponds to the systemic redshift of $z = 7.677$ set by the [C II] line. The golden area marks the channels used to optimize the S/N for the extraction. The blue and red lines and shaded areas indicate the Lyα Gaussian models and their confidence interval as labeled, arbitrarily rescaled in flux density. We adopted the optical radial velocity definition.

In the bottom panel of Figure 1, we show the ALMA Band 6 spectrum extracted in an aperture optimizing its signal-to-noise ratio (S/N). We identified a significant line emission consistent with being [C II] based on the identification of the Lyα transition (Section 2.1). We measure a spectroscopic redshift of $z_{\rm sys,[C\,II]} = 7.6771 \pm 0.0004$ from the Gaussian modeling of the detected line peaking at 219.027 GHz, in agreement with the photometric redshift estimates (Table 1).[6] We then collapsed the line detected channels and produced a [C II] velocity-integrated line map (Figure 2), where the peak pixel emission (per beam) is detected at $\sim 5.3\sigma$ significance. We also found that the [C II] line is spatially extended. We thus modeled the spatial profile of the [C II] emission in the velocity-integrated map with IMFIT as a single elliptical Gaussian, recovering the total flux over the channels maximizing the S/N (Figure 2).

[4] Program ID: U043M, PI: G. Illingworth.

[5] Program IDs: 2018.1.00236.S (PI: M. Stefanon), 2019.1.01634.L (PI: R. Bouwens).

[6] In parallel with our discovery of this line, an independent search by Bouwens et al. (2021b) also find a [C II] line for this source at 7.677 (with a nominal S/N of $\sim$7.8).

Table 1
Physical Properties of Y002

R.A. (J2000)	10:02:12.54 (150.55224056 deg)
Decl. (J2000)	+2:30:45.9 (2.51273892 deg)
$z_{\rm phot,C20}$[a]	$8.31^{+0.31}_{-0.58}$
$z_{\rm sys,[C\ II]}$	7.6771 ± 0.0004
$M_{\rm UV,1500}$	-21.95 ± 0.04
β	-2.58 ± 0.16
$\log(M_\star [M_\odot])$	$9.67^{+0.09}_{-0.15}$
$A_{\rm V}$ [mag]	$0.18^{+0.05}_{-0.05}$
Z [$Z_\odot$]	$0.29^{+0.18}_{-0.10}$
SFR(UV) [$M_\odot$ yr^{-1}]	22 ± 1
SFR(IR) [$M_\odot$ yr^{-1}]	<15
$L_{\rm Ly\alpha}$ [erg s^{-1}]	$(1.30 \pm 0.28) \times 10^{43}$
EW$_0$(Lyα) [Å]	24^{+5}_{-6}
$\sigma_{\rm vel}$(Lyα) [km s^{-1}]	248 ± 18
$\Delta v_{\rm Ly\alpha}$ [km s^{-1}]	480 ± 67
$\Delta x_{\rm Ly\alpha}$ [arcsec]	$0.64^{+0.11}_{-0.12}$
$S_{\rm [C\ II]}$ [Jy km s^{-1}]	(0.33 ± 0.07)
$L_{\rm [C\ II]}$ [$L_\odot$]	$(4.41 \pm 0.90) \times 10^8$
$L'_{\rm [C\ II]}$ [K km s^{-1} pc^2]	$(2.00 \pm 0.41) \times 10^9$
$\sigma_{\rm vel}$([C II]) [km s^{-1}]	63 ± 13
FWHM$_{\rm maj}$([C II]) [arcsec]	2.43 ± 0.63
FWHM$_{\rm min}$([C II]) [arcsec]	0.93 ± 0.44
$S_{1.44\ \rm mm}$ [μJy]	<27
$\log(L_{\rm IR,45K}/L_\odot)$	<11.03

Notes. Upper limits at 3σ.
[a] Photometric redshift from FARMER+LEPHARE in Weaver et al. (2022). An updated run with EAZY adopting more conservative uncertainties on IRAC fluxes similar to those used in the present work returns $z_{\rm phot,CI} = 7.77^{+0.35}_{-0.06}$. The estimate based on the "classical" aperture photometry is $z_{\rm phot,CI} = 7.69^{+1.06}_{-0.15}$.

The source is resolved and extended over $2\farcs43 \times 0\farcs93$ (deconvolved by the beam, Table 1). However, the [C II] map shows two separated and similarly bright peaks, which might suggest the possible existence of substructures. We thus attempted a double-Gaussian fit that returned an identical total [C II] flux estimate from two point-like sources separated by $\sim 1\farcs6$. Higher spatial resolutions and S/N will be necessary to confirm and investigate possible clumping.

We did not detect any dust continuum emission from Y002, as also previously reported by Schouws et al. (2022) based on slightly shallower observations from a pilot program for the REBELS survey. We, thus, set a 3σ upper limit of 27 μJy beam^{-1} at (observed) 1.44 mm. Given the large beam size, this is computed as the pixel rms in the continuum map in units of Jy beam^{-1} obtained by combining all the existing observations at these wavelengths.

2.3. Photometry

We extracted the photometry in the Y, J, H, and $K_{\rm s}$ bands from the UltraVISTA DR4 and the four Spitzer/IRAC channels from the latest reprocessed images (Weaver et al. 2022) with the custom code GOLFIR[7] (V. Kokorev & G. Brammer 2022, in preparation). The code uses priors from the highest spatial resolution imaging available to iteratively model and deblend the IRAC photometry. In Figure 3, we show the cutouts in optical to near-IR bands and a comparison between our photometry and that of the COSMOS2020 catalog extracted with THE FARMER (J. R. Weaver et al. 2022, in preparation). Generally, the two photometric sets are in good agreement, with the exception of the more conservative uncertainties on the IRAC fluxes that we adopt here.

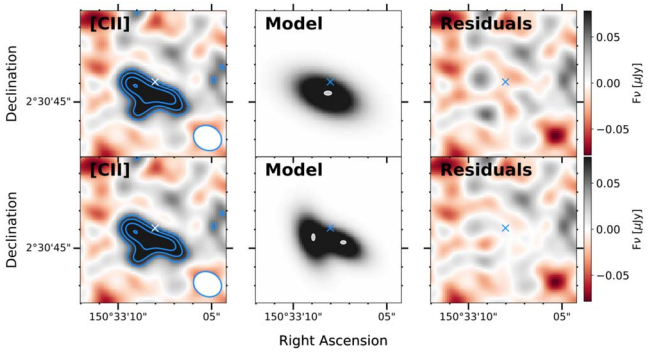

Figure 2. Modeling of the [C II] emission with single (top) and double (bottom) elliptical Gaussians. The cross shows the location of the rest-frame UV and optical emission. The white ellipses show the locations of the peaks of the modeled [C II] emission and their uncertainties. Blue lines in the left panels show 2σ–5σ contours. The images are color-scaled within $\pm 3\times$ rms.

We modeled our custom photometry with BAGPIPES (Carnall et al. 2018) following the approach described in Strait et al. (2021) (Figure 3). We adopted the Binary Population and Spectral Synthesis templates (BPASS; Eldridge & Stanway 2009) and included nebular continuum and emission lines computed with CLOUDY (Ferland et al. 2017), leaving the ionization parameter free to vary in a range of $\log(U) = [-4, -1]$. We used a broken power-law initial mass function with $\alpha = -2.35$ between 0.5–300 $M_\odot$ and $\alpha = -1.3$ at 0.1–0.5 $M_\odot$.[8] We used a flexible exponential star formation history able to rise, decline, or stay constant, along with a Calzetti et al. (2000) dust attenuation law ($A_{\rm V} = 0$–3), where twice as much dust is assigned to H II regions as in the diffuse ISM in the first 10 Myr. We left the metallicity as a free parameter ($Z = 0.005$–$5\ Z_\odot$), but fixed the redshift to its spectroscopic value $z_{\rm sys,[C\ II]}$. A detailed description of the modeling, its biases, and systematic uncertainties can be found in Strait et al. (2021).

The best-fit parameters are reported in Table 1. From the best-fit model, we also derived the continuum emission underlying the Lyα line because no detectable trace was found in the MOSFIRE spectrum. This estimate is consistent with that derived from the observed continuum in the J band (the closest filter completely redward of the Lyα break) and by assuming a flat constant spectrum in F_ν. We further computed the unobscured SFR from the rest-frame UV luminosity at 1500 Å as $\rm SFR_{UV}[M_\odot\ yr^{-1}] = 8.24 \times 10^{-29}\ L_{\nu,UV}$ [erg s^{-1} Hz^{-1}] (Schaerer et al. 2020). Moreover, we derived an upper limit on the obscured SFR from the total infrared luminosity $L_{\rm IR(8–1000\ \mu m)}$ obtained by rescaling a modified blackbody curve with a dust temperature of $T_{\rm dust} = 45$ K and a $\beta_{\rm IR} = 1.5$ power-law exponent to the continuum emission at $\sim 160\ \mu$m rest frame, modeling the effect of the cosmic microwave background as in da Cunha et al. (2013). We then applied the conversion $\rm SFR_{IR}\ [M_\odot\ yr^{-1}] = 1.4 \times 10^{-10} L_{IR}\ [L_\odot]$. For a dust mass absorption coefficient of $k_0 = 8.94$ g cm^2 g^{-1} at 158 μm (Hirashita et al. 2014), the 3σ upper limit on the continuum detection corresponds to a dust mass of

[7] https://github.com/gbrammer/golfir

[8] The fiducial BPASS IMF has a similar shape to that of Chabrier (2003) or Kroupa (2001). The resulting mass-to-light ratio tracks well with the value for the Bruzual & Charlot (2003) single population synthesis models for ages of <6 Gyr (Figure 7 in Stanway & Eldridge 2018).

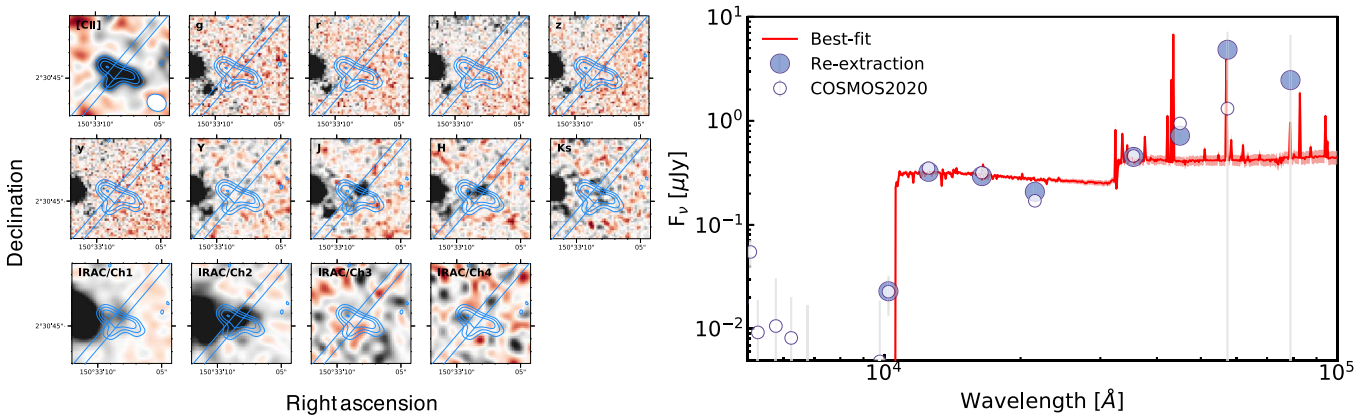

Figure 3. Left: $8'' \times 8''$ cutouts of ALMA/[C II] and optical to near-IR images from the COSMOS2020 catalog (Weaver et al. 2022). The cutouts are color-scaled within $\pm 3\times$ rms in each image and are aligned N–E. The blue contours and slanted lines show the ALMA/[C II] 2σ–5σ levels and the Keck/MOSFIRE slit orientation. The size of the ALMA beam is shown in the first cutout. Right: best-fit photometric model of the SED with BAGPIPES at fixed $z = 7.677$ and its uncertainty (red line and shaded area). Empty and filled blue circles mark the photometry from the COSMOS2020 catalog (Weaver et al. 2022) and our custom re-extraction.

$M_{\rm dust} < 10^{6.9}\,M_\odot$. The ratio of $L_{\rm [C\,II]}$ to its underlying dust continuum luminosities is consistent with the upper end of the distribution of the 158 μm continuum detected sources in the REBELS sample (Sommovigo et al. 2022).

3. Results and Discussion

3.1. Lyα and [C II] Offsets

In Figure 1, the velocity offset of the Lyα line with respect to the systemic redshift set by the [C II] emission can be fully appreciated. The peak of the Gaussian profile is redshifted by $\Delta v_{\rm Ly\alpha} \sim 500$ km s^{-1} from $z_{\rm sys,[C\,II]}$ with a significant high-velocity tail extending up to $\sim$1000 km s^{-1}.[9] This value is $\sim 3.5\times$ higher than the observed average offset for similarly bright objects at $z \sim 6$–7 ($\sim$150–200 km s^{-1}, Pentericci et al. 2016; Matthee et al. 2019) and the recent modeling of the $M_{\rm UV}$–$\Delta v_{\rm Ly\alpha}$ relation at $z = 7$–8 by Mason et al. (2018b), computed without including outflow models explicitly (Figure 4). However, $\Delta v_{\rm Ly\alpha}$ is consistent with the average estimate for $M_{\rm UV} < -22$ galaxies at $z > 6$ reported by Endsley et al. (2022), including four objects from the REBELS survey,[10] similar to CLM1 at $z = 6.17$ (Willott et al. 2015), but lower than what reported for B14-65666 at $z = 7.15$ ($\Delta v_{\rm Ly\alpha} \sim 770$ km s^{-1}, Hashimoto et al. 2019). Similar to CLM1, but at odds with B14-65666, in the case of Y002, the velocity offset does not pair with a remarkably low value of the EW$_0$(Lyα) and high $L_{\rm [C\,II]}$, despite the similar $M_{\rm UV}$ (Table 1). Quite the opposite: Y002 is among the strongest UV-bright Lyα emitters at $z > 6$ with an EW$_0$(Lyα) $= 24^{+5}_{-6}$ Å (Figure 4). The velocity offset is consistent with the average for LBGs at similar magnitudes at $z \sim 2$–3.5 (Erb et al. 2004; Steidel et al. 2010; Willott et al. 2015; Marchi et al. 2019; Cassata et al. 2020).

We also report a spatial offset of $\Delta x_{\rm Ly\alpha} = 0\farcs64^{+0.11}_{-0.12}$ ($3.16^{+0.54}_{-0.59}$ kpc) between the peaks of the rest-frame UV stellar light—colocated with the Lyα emission—and that of the [C II] emission. Larger spatial offsets ($\sim 0\farcs75$–$1''$) would be measured from the peaks of the possible substructures in the [C II] map, if confirmed (Figure 2). At the current spatial resolution at rest-frame UV and FIR wavelengths, an overlap between the stellar and cold gaseous components remains.

3.2. A Hint of Complex Geometry

The spatial offset and the large Lyα velocity shift could be explained if we considered Y002 to be composed of multiple merging clumps with different physical properties (Carniani et al. 2018; Hashimoto et al. 2019). The lack of Lyα photons percolating from the region close to the peak of the [C II] emission could be explained by a large amount of neutral hydrogen resonantly trapping the Lyα light and a minimal mass of dust absorbing it. Following Heintz et al. (2021) and assuming that [C II] traces the H I mass in the ISM at $z > 6$, we derived a total $\log(M_{\rm HI}/M_\odot)_{Z=0.3Z_\odot} = (10.58 \pm 0.17)$ for a representative metallicity of $Z = 0.3\,Z_\odot$ and including the uncertainties on the calibration. The H I mass is $\sim 8\times$ higher than $M_\star$ in Y002 as a global system, suggesting the existence of large neutral gas reservoirs. Under these assumptions, we could consider this ratio as a lower limit consistent with the extrapolation of the $M_{\rm H\,I}/M_\star - z$ trend derived up to $z \sim 6$ (Heintz et al. 2021, 2022 in preparation). We further derived a column density of $N_{\rm HI} \sim 10^{22.7\pm0.3}$ cm^{-2} within an effective ellipse of 43.4 ± 23.8 kpc^2 enclosing half of the total [C II] luminosity as estimated from the Gaussian modeling (half-light semiaxes $a_{\rm maj,min} = {\rm FWHM}_{\rm maj,min}/2$). This $N_{\rm H\,I}$ estimate is consistent with the values in the high-density tail from direct observations of gamma-ray bursts in star-forming galaxy cores up to $z \sim 4$–5 (Tanvir et al. 2019). These column densities are challenging for the predictions of a simple expanding shell model (Verhamme et al. 2015). In this case, the Lyα emission would not be able to escape from the [C II]-emitting dense H I region even with the low amount of dust expected Y002 from the upper limit on the continuum detection (Section 2.3). If some of the observed Lyα light were resonantly scattered from the [C II] clump and escaping at high velocities, we would

[9] For the sake of completeness, we retrieve $\Delta v_{\rm Ly\alpha} = (182 \pm 57)$ km s^{-1} from the skewed Gaussian model. The (nonparametric) first moment computed over the wavelength bins, where $F_\lambda > 1\%$ of the peak derived from the best-fit Gaussian model ($\lambda \in [10535.3,\ 10587.4]$ Å), and weighted by the S/N to reduce the impact of noise peaks is 432 km s^{-1}.

[10] The average estimate from Endsley et al. (2022) assumes $\Delta v_{\rm Ly\alpha} = 504 \pm 52$ km s^{-1} for WMH5(-B) at $z = 6.07$, in lieu of the 265 ± 52 km s^{-1} value for WMH5(-A) listed by Matthee et al. (2019) and adopted here (Willott et al. 2015).

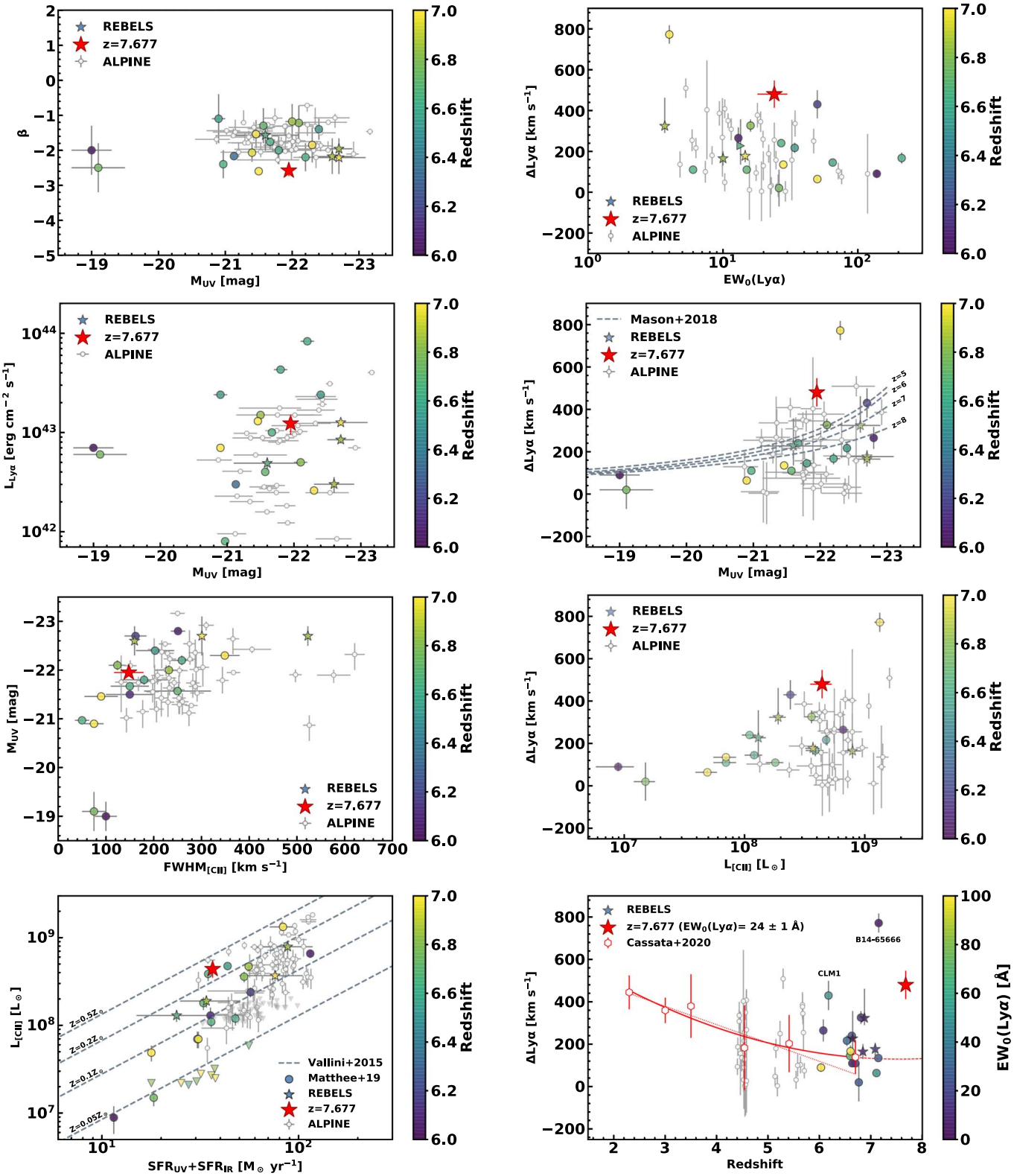

Figure 4. The location of Y002 in the plane of observables. Left column: $M_{\rm UV}$ vs. β; $M_{\rm UV}$ vs. $L_{\rm Ly\alpha}$; FWHM$_{[\rm C\,II]}$ vs. $M_{\rm UV}$; SFR$_{\rm UV}$ + SFR$_{\rm IR}$ vs. $L_{[\rm C\,II]}$. Right column: EW$_0$(Lyα) vs. $\Delta v_{\rm Ly\alpha}$; $M_{\rm UV}$ vs. $\Delta v_{\rm Ly\alpha}$; $L_{[\rm C\,II]}$ vs. $\Delta v_{\rm Ly\alpha}$; redshift vs. $\Delta v_{\rm Ly\alpha}$. In each panel, the red filled star marks the location of Y002. The filled circles show the compilation of $z \sim 6$–7 Lyα and [C II] emitters from Matthee et al. (2019) and Hashimoto et al. (2019) color-coded as labeled. Filled stars indicate the galaxies from the REBELS survey with Lyα detection presented in Endsley et al. (2022) (β values from Bouwens et al. 2021b). Sources from the ALPINE survey at $z \sim 4$–6 are shown in gray (Béthermin et al. 2020; Cassata et al. 2020; Faisst et al. 2020). The dashed lines in the bottom-left panel mark the SFR–$L_{[\rm C\,II]}$ relation as a function of metallicity as in Vallini et al. (2015). The ones in the $M_{\rm UV}$–$\Delta v_{\rm Ly\alpha}$ panel show the median relation as a function of redshift in Mason et al. (2018a). The red symbols and lines in the bottom-right panel indicate the average values and the best-fit linear and parabolic trends as in Cassata et al. (2020).

expect a simultaneous decrease in $EW_0(Ly\alpha)$, which is not observed. Moreover, the overlap between the Lyα and UV emission lends support to an in situ production scenario. Different levels of metal enrichment, hardness of the ambient radiation field, and dust extinction could then concur to explain the spatial offsets (Carniani et al. 2018).

This is a simple calculation providing an average and approximate estimate of the H I column density from [C II], critically depending on the metallicity of the ISM. Here we adopted the loose constraint from the SED modeling of the UV-bright component, but indirect arguments support this choice. On the one hand, discounting very high dust temperatures, the nondetection of continuum emission suggests $Z < Z_{\odot}$, as one could expect at such high redshifts (but see Watson et al. 2015). On the other hand, lower metallicities and extreme $M_{\rm H\,I}$ are disfavored by the approximate estimate of the dynamical mass $M_{\rm dyn} \approx 1.16 \times 10^5 v_{\rm circ}^2 D \sim 3 \times 10^{10} M_{\odot}$ that we computed from the [C II] emission (Wang et al. 2013). Here, $v_{\rm circ} = 0.75\,{\rm FWHM}_{\rm [C\,II]}/\sin(i)$ is the maximum circular velocity of the gas in km s^{-1} assuming a rotating disk geometry for the [C II]-emitting component, $D = 1.5 \times {\rm FWHM}_{\rm maj}$ the size in kiloparsecs, and $i = \cos^{-1}(a_{\rm min}/a_{\rm maj})$ is the disk inclination from the minor/major axis ratio.

3.3. A Bright System Deep in the Reionization Epoch

The best-fit SED modeling at fixed $z_{\rm sys,[C\,II]}$ suggests that Y002 is a relatively massive ($\log(M_{\star}/M_{\odot}) = 9.67^{+0.09}_{-0.15}$) and UV-bright system (2× brighter than $M_{\rm UV}^{\star}$ at $z = 7$–8; Bouwens et al. 2021a). For the sake of comparison with the literature and considering Y002 as a single system, the SFR(UV)+SFR(IR) and $L_{\rm [C\,II]}$ estimates place it on the upper end of the empirical relation among these quantities observed across redshifts (Figure 4, De Looze et al. 2014; Vallini et al. 2015; Schaerer et al. 2020). Also, Y002 does not deviate significantly from the correlations observed among $M_{\rm UV}$, β slope, FWHM([C II]), and $L_{\rm Ly\alpha}$ (Figure 4).

The large velocity offset between the Lyα peak and the systemic redshift is what distinguishes Y002 compared with most of the known high-redshift galaxies, in a similar fashion to the systems reported by Willott et al. (2015) and Hashimoto et al. (2019). Empirical correlations among $\Delta v_{\rm Ly\alpha}$ and $EW_0(Ly\alpha)$, $L_{\rm [C\,II]}$, and $M_{\rm UV}$ appear to be in place at $z > 6$ based on composite literature compilations (Hashimoto et al. 2019; Endsley et al. 2022). Because Lyα is a resonant line, its velocity offset can be interpreted as owing to large H I column densities (paired with low $EW_0(Ly\alpha)$) and as a signature of outflowing material (Verhamme et al. 2006, 2015). The empirical correlations among $\Delta v_{\rm Ly\alpha}$ and $L_{\rm [C\,II]}$ and $M_{\rm UV}$ could just reflect larger $N_{\rm H\,I}$ and stronger SFR-driven outflows in bright [C II] and UV emitters, respectively (Hashimoto et al. 2019). Discounting luminosity selection effects, the absence of sources detected at high $\Delta v_{\rm Ly\alpha}$ for low $L_{\rm [C\,II]}$ and faint $M_{\rm UV}$ would be explained by the fact that Lyα photons can escape closer to their rest-frame wavelength. However, in Figure 4 we show that the addition of the ALPINE sample of main-sequence galaxies at $z \sim 4$–6 does not fully support these findings. While this could be due to the different selection functions (Harikane et al. 2020), a transition around $z \sim 6$ could be expected due to the increasing IGM neutral fraction at $z > 6$. In addition, extremely large $\Delta v_{\rm Ly\alpha}$ could simply reflect the existence of merging substructures or galaxies, calling into question the physical association of [C II]-, UV-, or Lyα-emitting clumps, for which such correlations might not a priori exist.

3.4. A Large Reionization Patch?

The existence of an ionized bubble around Y002 could facilitate the escape of Lyα photons. The detection of strong Lyα emission ($EW_0(Ly\alpha) = 24^{+5}_{-6}$ Å) might, in fact, suggest the existence of such a large patch of reionization (Stark et al. 2017; Leonova et al. 2021). The measured $EW_0(Ly\alpha)$ is 2× larger than the median values for galaxies with $M_{\rm UV} < -20.4$ in the field at $z \sim 7$, but consistent with the value reported for an overdensity of emitters at a similar redshift (Endsley & Stark 2022). However, a model of the observed $EW_0(Ly\alpha)$ distribution in an inhomogeneously reionizing IGM by Mason et al. (2018a) (their Figure 7) returns a probability of $5.8^{+1.0}_{-1.1}$% to detect a galaxy with $M_{\rm UV} = -22$ and such large $EW_0(Ly\alpha)$ at $z = 7.6$, given the current constraints on the IGM neutral fraction at that redshift ($x_{\rm H\,I} = 0.74^{+0.07}_{-0.06}$; Hoag et al. 2019; Mason et al. 2019). This points once more to the prominent role of the large Lyα velocity offset in facilitating photon escape. If future observations confirmed $\Delta v_{\rm Ly\alpha}$ of the order of ∼500 km s^{-1} (Table 1), it would be potentially sufficient to explain the emission without invoking the transparency of the surrounding IGM over large scales (Endsley et al. 2022).

4. Conclusions

We reported the archival discovery of strong Lyα emission from a UV-bright (2× brighter than $M_{\rm UV}^{\star}$) system spectroscopically confirmed by its [C II] emission detected with ALMA at $z = 7.677$. The peaks of the Lyα and [C II] emission appear offset both spatially (∼3 kpc) and in velocity ($\Delta v_{\rm Ly\alpha} \sim 500$ km s^{-1}), with the emission from the recombining hydrogen atoms being coincident with the rest-frame UV stellar light.

The velocity offset is among the largest reported so far and 3.5× higher than the average at $z \sim 6$–7 while being paired with a large $EW_0(Ly\alpha) = 24^{+5}_{-6}$ Å. The spatial and velocity offsets hint at the existence of a complex structure and merging subunits. The distribution of large amounts of H I gas, coupled with a minimal amount of dust (as derived from the 3σ upper limit on the continuum emission at 160 μm rest-frame, $M_{\rm dust} < 10^{6.9}$ $M_{\odot}$), could help explain the observed spatial offsets. By assuming that [C II] primarily traces H I, we estimated $\log(M_{\rm H\,I}/M_{\odot})_{Z=0.3Z_{\odot}} \sim 10.6$, ∼8× larger than the $M_{\star}$ estimated for Y002 as a single system. For a simplified uniform distribution of the measured size of the system, we derive an approximate estimate of $N_{\rm H\,I}$ in excess of $10^{22.5}$ cm^{-2}, enough to trap and absorb the Lyα emission from the [C II]-emitting clump. Escape at a very high velocity (possibly suggested by the observed $\Delta v_{\rm Ly\alpha} \sim 500$ km s^{-1}) would be hardly compatible with the large $EW_0(Ly\alpha)$ that we estimate.

As a single system, Y002 stands out compared with other high-redshift systems for the large Lyα velocity offset and $EW_0(Ly\alpha)$. The latter might be a common feature among UV-bright galaxies at $z \sim 6$–7, as supported by the observed correlations between $\Delta v_{\rm Ly\alpha}$, $L_{\rm [C\,II]}$ ($\propto M_{\rm H\,I}$), and $M_{\rm UV}$ ($\propto {\rm SFR}_{\rm UV}$). However, such correlations are not immediately evident when including samples at $z \sim 4$–5. Moreover, extremely large $\Delta v_{\rm Ly\alpha}$ might result from spatially disconnected regions, challenging the strength of the observed correlations in the absence of high-resolution observations. Finally, such a

large $EW_0(Ly\alpha)$ from a system as bright as $M_{UV} = -22$ has a relatively low probability of being observed of ∼5% at $z = 7.6$, given the current constraints on the IGM neutral fraction. This independently suggests the central role of outflows in facilitating the escape of Lyα photons, besides the possible existence of an ionized bubble around this system.

Several aspects deserve to be clarified in future work. High-resolution and deeper ALMA [C II] observations are necessary to unambiguously confirm and describe the clumpy substructure of Y002, currently only suggested by our modeling of the [C II] map. In addition, the emission of several rest-frame optical lines from the ionized gas phase (oxygen, hydrogen) is within reach of the James Webb Space Telescope. High-resolution measurements could unambiguously determine the spatial distribution, velocity offset, Lyα escape fractions, metallicities, and ionization parameter of the ionized phases and the stellar component.

We acknowledge the constructive comments from the anonymous referee that improved the content and presentation of the results. We warmly thank Paolo Cassata for providing data from his work, Rychard Bouwens for his suggestions about the REBELS survey, and Ivo Labbé for his useful comments on this analysis. The Cosmic Dawn Center (DAWN) is funded by the Danish National Research Foundation under grant No. 140. F.V. and K.E.H. acknowledge support from the Carlsberg Foundation under grants CF18-0388 and CF21-0103. K.E.H. acknowledges support by a Postdoctoral Fellowship Grant (217690–051) from The Icelandic Research Fund. S.F. and D.W. are supported by Independent Research Fund Denmark grant DFF–7014-00017. C.M. acknowledges support by the VILLUM FONDEN under grant 37459. S.T. and J.R.W. acknowledge support from the European Research Council (ERC) Consolidator Grant funding scheme (project ConTExt, grant No. 648179). Some of the data presented herein were obtained at the W. M. Keck Observatory, which is operated as a scientific partnership among the California Institute of Technology, the University of California, and the National Aeronautics and Space Administration. The Observatory was made possible by the generous financial support of the W. M. Keck Foundation. The authors wish to recognize and acknowledge the very significant cultural role and reverence that the summit of Maunakea has always had within the indigenous Hawaiian community. We are most fortunate to have the opportunity to conduct observations from this mountain. This paper makes use of the following ALMA data: 2018.1.00236.S, 2019.1.01634.L. ALMA is a partnership of ESO (representing its member states), NSF (USA), and NINS (Japan), together with NRC (Canada), MOST and ASIAA (Taiwan), and KASI (Republic of Korea), in cooperation with the Republic of Chile. The Joint ALMA Observatory is operated by ESO, AUI/NRAO and NAOJ.

ORCID iDs

Francesco Valentino https://orcid.org/0000-0001-6477-4011
Gabriel Brammer https://orcid.org/0000-0003-2680-005X
Seiji Fujimoto https://orcid.org/0000-0001-7201-5066
Kasper E. Heintz https://orcid.org/0000-0002-9389-7413
John R. Weaver https://orcid.org/0000-0003-1614-196X
Victoria Strait https://orcid.org/0000-0002-6338-7295
Katriona M. L. Gould https://orcid.org/0000-0003-4196-5960
Charlotte Mason https://orcid.org/0000-0002-3407-1785
Darach Watson https://orcid.org/0000-0002-4465-8264
Peter Laursen https://orcid.org/0000-0003-4207-0245
Sune Toft https://orcid.org/0000-0003-3631-7176

References

Béthermin, M., Fudamoto, Y., Ginolfi, M., et al. 2020, A&A, 643, A2
Bouwens, R. J., Oesch, P. A., Stefanon, M., et al. 2021a, AJ, 162, 47
Bouwens, R. J., Smit, R., Schouws, S., et al. 2021b, arXiv:2106.13719
Bowler, R. A. A., Dunlop, J. S., McLure, R. J., & McLeod, D. J. 2017, MNRAS, 466, 3612
Bruzual, G., & Charlot, S. 2003, MNRAS, 344, 1000
Calzetti, D., Armus, L., Bohlin, R. C., et al. 2000, ApJ, 533, 682
Capak, P. L., Carilli, C., Jones, G., et al. 2015, Natur, 522, 455
Carnall, A. C., McLure, R. J., Dunlop, J. S., & Davé, R. 2018, MNRAS, 480, 4379
Carniani, S., Maiolino, R., Amorin, R., et al. 2018, MNRAS, 478, 1170
Cassata, P., Morselli, L., Faisst, A., et al. 2020, A&A, 643, A6
Chabrier, G. 2003, PASP, 115, 763
da Cunha, E., Groves, B., Walter, F., et al. 2013, ApJ, 766, 13
Dayal, P., & Ferrara, A. 2018, PhR, 780, 1
De Looze, I., Cormier, D., Lebouteiller, V., et al. 2014, A&A, 568, A62
Eldridge, J. J., & Stanway, E. R. 2009, MNRAS, 400, 1019
Endsley, R., & Stark, D. P. 2022, MNRAS, 511, 6042
Endsley, R., Stark, D. P., Bouwens, R. J., et al. 2022, arXiv:2202.01219
Erb, D. K., Steidel, C. C., Shapley, A. E., Pettini, M., & Adelberger, K. L. 2004, ApJ, 612, 122
Faisst, A. L., Schaerer, D., Lemaux, B. C., et al. 2020, ApJS, 247, 61
Ferland, G. J., Chatzikos, M., Guzmán, F., et al. 2017, RMxAA, 53, 385
Harikane, Y., Ouchi, M., Inoue, A. K., et al. 2020, ApJ, 896, 93
Harikane, Y., Ouchi, M., Shibuya, T., et al. 2018, ApJ, 859, 84
Hashimoto, T., Inoue, A. K., Mawatari, K., et al. 2019, PASJ, 71, 71
Heintz, K. E., Watson, D., Oesch, P. A., Narayanan, D., & Madden, S. C. 2021, ApJ, 922, 147
Hirashita, H., Ferrara, A., Dayal, P., & Ouchi, M. 2014, MNRAS, 443, 1704
Hoag, A., Bradač, M., Huang, K., et al. 2019, ApJ, 878, 12
Horne, K. 1986, PASP, 98, 609
Kroupa, P. 2001, MNRAS, 322, 231
Le Fèvre, O., Béthermin, M., Faisst, A., et al. 2020, A&A, 643, A1
Leonova, E., Oesch, P. A., Qin, Y., et al. 2021, arXiv:2112.07675
Loeb, A., & Barkana, R. 2001, ARA&A, 39, 19
Marchi, F., Pentericci, L., Guaita, L., et al. 2019, A&A, 631, A19
Mason, C. A., Naidu, R. P., Tacchella, S., & Leja, J. 2019, MNRAS, 489, 2669
Mason, C. A., Treu, T., de Barros, S., et al. 2018a, ApJL, 857, L11
Mason, C. A., Treu, T., Dijkstra, M., et al. 2018b, ApJ, 856, 2
Matthee, J., Sobral, D., Boogaard, L. A., et al. 2019, ApJ, 881, 124
McLean, I. S., Steidel, C. C., Epps, H. W., et al. 2012, Proc. SPIE, 8446, 84460J
McMullin, J. P., Waters, B., Schiebel, D., Young, W., & Golap, K. 2007, in ASP Conf. Ser. 376, Astronomical Data Analysis Software and Systems XVI, ed. R. A. Shaw, F. Hill, & D. J. Bell (San Francisoc, CA: ASP), 127
Pentericci, L., Carniani, S., Castellano, M., et al. 2016, ApJL, 829, L11
Schaerer, D., Ginolfi, M., Béthermin, M., et al. 2020, A&A, 643, A3
Schouws, S., Stefanon, M., Bouwens, R. J., et al. 2022, ApJ, 928, 31
Sommovigo, L., Ferrara, A., Pallottini, A., et al. 2022, MNRAS, Advanced Access
Stanway, E. R., & Eldridge, J. J. 2018, MNRAS, 479, 75
Stark, D. P., Ellis, R. S., Charlot, S., et al. 2017, MNRAS, 464, 469
Stefanon, M., Labbé, I., Bouwens, R. J., et al. 2017, ApJ, 851, 43
Stefanon, M., Labbé, I., Bouwens, R. J., et al. 2019, ApJ, 883, 99
Steidel, C. C., Erb, D. K., Shapley, A. E., et al. 2010, ApJ, 717, 289
Strait, V., Bradač, M., Coe, D., et al. 2021, ApJ, 910, 135
Tanvir, N. R., Fynbo, J. P. U., de Ugarte Postigo, A., et al. 2019, MNRAS, 483, 5380
Vallini, L., Gallerani, S., Ferrara, A., Pallottini, A., & Yue, B. 2015, ApJ, 813, 36
Verhamme, A., Orlitová, I., Schaerer, D., & Hayes, M. 2015, A&A, 578, A7
Verhamme, A., Schaerer, D., & Maselli, A. 2006, A&A, 460, 397
Wang, R., Wagg, J., Carilli, C. L., et al. 2013, ApJ, 773, 44
Watson, D., Christensen, L., Knudsen, K. K., et al. 2015, Natur, 519, 327
Weaver, J. R., Kauffmann, O. B., Ilbert, O., et al. 2022, ApJS, 258, 11
Willott, C. J., Carilli, C. L., Wagg, J., & Wang, R. 2015, ApJ, 807, 180